ISSN 1063-7729, Astronomy Reports, 2024, Vol. 68, No. 12, pp. 1457–1469. © Pleiades Publishing, Ltd., 2024.

Spectroscopic Binary Cepheid AU Peg in the Gaia DR3 Epoch: Effect of Ellipsoidality, Mass, and Evolutionary Status

A. S. Rastorguev[a,b,*], M. V. Zabolotskikh[b], and N. A. Gorynya[c,b]

[a] *Lomonosov Moscow State University, Moscow, 119991 Russia*

[b] *Sternberg Astronomical Institute, Lomonosov Moscow State University, Moscow, 119234 Russia*

[c] *Institute of Astronomy of the Russian Academy of Sciences, Moscow, 119017 Russia*

**e-mail: alex.rastorguev@gmail.com*

Received November 20, 2024; revised December 25, 2024; accepted December 25, 2024

Abstract—The physical characteristics and evolutionary status of the spectroscopic binary Cepheid AU Peg, usually classified as a BL Her variable, is revised. Taking into account previously unpublished radial velocity measurements made with a radial velocity meter (RVM), the parameters of the relative orbit of the Cepheid and its companion are refined. Based on the available radial velocity measurements and photometric observations, a number of estimates of the Cepheid's pulsating radius are made. Based on 74 new radial velocity measurements made in the period JD2453930–2459490 virtually simultaneously with the Gaia DR3 photometric observations (44 brightness measurements in the period JD256962–2457877), the mean radius of AU Peg is determined by the pulsating photosphere method equal to $(16.0 \pm 0.6)\ R_\odot$; the amplitude of radius variations is about 0.7 $R_\odot$. For the first time, 2% brightness variations are found for a spectroscopic binary Cepheid in the G band with a half orbital period, the phases of which are clearly synchronized with the phases of the orbital motion (conjunctions and quadratures) and can be interpreted as a manifestation of the ellipsoidality effect of the main component filling the Roche sphere at 60–70%. The orbit of the binary system calculated on the basis of astrometric data from Gaia DR3 and radial velocities is limited by a torus with a thickness of $|z| \leq 300$ pc and inner and outer radii equal to 7.2 and 8.8 kpc, respectively, while the vertical velocity lies within $|V_z| \leq 18$ km/s. Based on the kinematics and abundance of heavy elements, AU Peg can certainly be classified as a representative of the typical population of a thin disk of moderate (~1–3 Gyr) age, which completely excludes its classification as a BL Her variable. The Cepheid, which current mass, as follows from the magnitude of ellipsoidality, does not exceed $\sim(0.85 \pm 0.05)\ M_\odot$, is at the evolutionary stage after the mass exchange in the subgiant phase with a companion - a main-sequence star, which is currently significantly more massive than the Cepheid.

Keywords: binary and multiple stars, AU Peg, stellar evolution, fundamental parameters of stars

DOI: 10.1134/S1063772925701409

1. INTRODUCTION

Spectroscopic binaries Cepheids are one of the most important classes of binary star systems. Long series of precision radial velocity measurements allow us to reliably separate the contributions of orbital motion and pulsations, determine the parameters of the relative orbit of the Cepheid and companion, find a lower estimate of the mass of the companion, and, based on the pulsation curve and photometry, determine the radius of the Cepheid using modern versions of the pulsating photosphere method. With separate spectroscopic and photometric data on the companion, it is also possible to impose constraints on the Cepheid mass itself [1, 2]. Thus, a comprehensive study of spectroscopic binary Cepheids provides a unique opportunity to clarify their evolutionary status, the parameters of the widely used period-luminosity relation for Cepheids, and to obtain important information about the physical processes responsible for the formation of massive binary stars in star-forming regions.

It is for these reasons that spectroscopic binary Cepheids became the main target of a long-term program of mass systematic radial velocity measurements of Cepheids in the northern sky using a correlation spectrograph—the Radial Velocity Meter (RVM) [3], carried out by the Institute of Astronomy of the Russian Academy of Sciences (INASAN) and the Sternberg State Astronomical Institute of Lomonosov Moscow State University in 1987–2022. Some of the results of this program, which in total contain about 14000 radial velocity measurements with a characteristic accuracy of about 0.3–0.5 km/s, were published earlier [4–6], and the data from the last 20 years of observations will be published in this and our subse-

Table 1. Catalog of new radial velocity measurements of AU Peg. Julian dates of measurements, radial velocities V_r and their uncertainties eV_r are given

JD-2400000	V_r, km/s	eV_r, km/s	JD-2400000	V_r, km/s	eV_r, km/s	JD-2400000	V_r, km/s	eV_r, km/s
53930.510	37.70	0.70	55800.525	28.33	0.81	56964.307	27.66	0.45
53932.562	57.49	1.42	55802.524	47.61	0.75	56966.262	27.52	0.46
53933.554	33.33	0.59	55809.502	15.04	0.52	56971.203	48.51	1.22
53943.540	−3.58	0.59	55810.488	−12.55	0.88	56971.212	33.47	0.65
53974.500	7.10	0.48	55861.313	−0.79	0.62	57269.479	−24.54	0.74
53975.492	31.37	0.59	55869.314	−22.48	0.35	57286.419	51.23	1.98
53977.402	32.55	0.66	55870.298	−34.60	0.77	57300.397	24.35	0.58
53979.400	31.57	0.64	55870.318	−42.18	1.20	57303.392	19.08	1.21
53982.473	50.18	0.71	55872.290	−27.40	0.86	57327.299	−8.36	0.56
53990.488	45.72	0.96	55873.292	−54.39	0.43	57647.494	−12.72	0.71
55492.298	−17.96	0.38	56156.538	−2.01	0.36	57648.520	−22.69	0.81
55493.350	−8.01	0.39	56158.523	3.12	0.36	57653.407	9.43	0.68
55494.368	−34.10	0.49	56164.505	45.45	0.66	57697.281	−44.28	0.41
55500.372	−34.94	0.53	56164.525	34.81	1.33	57997.506	1.25	0.65
55501.242	−55.96	0.39	56175.488	34.52	0.56	58030.421	13.98	0.72
55502.326	−45.66	0.31	56176.481	42.87	0.74	58362.511	47.63	1.01
55503.355	−35.78	0.61	56177.504	18.51	0.70	58730.451	45.58	0.89
55504.302	−54.27	0.35	56178.396	33.10	0.40	58730.477	43.00	0.95
55505.311	−37.71	0.72	56223.331	36.66	0.41	58736.455	41.60	1.43
55506.259	−58.62	0.63	56240.280	−23.34	0.43	58798.321	−4.08	0.81
55795.476	33.76	1.27	56534.490	4.47	0.72	58800.321	−20.07	0.90
55796.493	40.65	0.44	56889.459	−23.28	0.33	59134.392	−31.59	0.90
55797.525	54.47	0.85	56909.464	35.56	0.45	59488.399	14.19	1.16
55798.507	33.42	0.55	56910.396	17.15	0.65	59490.419	3.14	0.55
55799.498	49.95	0.36	56911.469	34.61	0.37			

quent articles. The new radial velocity measurements of AU Peg are given in Table 1.

This paper presents new results from studying the unique spectroscopic binary Cepheid AU Peg (BD+ 174572 = Gaia DR3 1785352625740690432), discovered by Hoffmeister [7], who labeled it as a short-period variable ($P_{pls} \approx 2.4^d$). The first photoelectric observations of this Cepheid were performed in [8]. Subsequently, AU Peg was classified as a type II Cepheid (T2), or more precisely, a subclass of BL Her. As a rule, this class of variable stars includes stars that are at the evolutionary stage of crossing the instability strip on the way to the asymptotic giant branch. The authors of [9–11], who studied variable stars in the Large Magellanic Cloud, Small Magellanic Cloud, and the Milky Way bulge based on observations within the OGLE project [12], attributed Cepheids with periods from 1 to 4–5 days to this type. The authors of [13] constructed pulsation models of stars at this stage for masses 0.5–0.65 $M_\odot$ and metallicities $Z = 0.0001$, 0.001, 0.004. In [14, 15], linear and nonlinear pulsation models were calculated for a wider range of masses (0.5–0.8 $M_\odot$), metallicities ($(-2.0 < [Fe/H] < 0.0)$, and luminosities (50–300 $L_\odot$).

The spectral binarity of AU Peg was reliably established in [16]; however, due to the small number of radial velocity measurements, the orbital period was estimated as $P_{orb} \le 50^d$. An important observation was made in the meantime: the spectral line H_α was systematically shifted to the blue region by an average of 25 km/s; a similar shift was also found for another T2 Cepheid of the same subclass, TX Del. The shift may be explained by gas outflow from the envelope of a low-mass star, pulsating with a velocity reaching 10 km/s. The presence of an envelope is confirmed by a small infrared excess [17] in the MIR range, corresponding to a gas temperature of about 500 K. The first reliable determination of the main orbital parameters was made in [18] from new spectral measurements. An almost modern value of the orbital period $P_{orb} \approx 53.3^d$ was obtained, but a rather large eccentricity $e \approx 0.12 \pm 0.04$ compared to the modern (almost zero) value. Three spectroscopic measurements of the

effective temperature in the range of 5300–5600 K, metallicity [Fe/H] ≈ 0.1±0.2, and surface acceleration $\log g \sim 2.0$ were made simultaneously, and a conclusion was made that AU Peg lies beyond the red boundary of the theoretical instability strip (see Fig. 4 in the cited article). As will be shown below, in [18, 19] the brightness of AU Peg is overestimated by approximately $1-1.5^m$ (V), which only strengthens the conclusion about the unusually red color of AU Peg. Another feature is the relatively large mass of the companion, estimated from the mass function, which led the authors of the cited article to the conclusion about the possible proximity of the star's radius to filling the Roche lobe. AU Peg is one of two known T2 stars with the shortest orbital periods of about 50^d, which suggests the possibility of a significant tidal influence of the companion on the star pulsations. These facts and assumptions are quite sufficient to consider AU Peg a very atypical representative of the BL Her type variables.

A number of widely differing estimates of the AU Peg radius were made using versions of the pulsating photosphere method after decomposing the radial velocity curve into the contributions of orbital motion and pulsations in [18] ($(16.5 \pm 1.0)\ R_\odot$), [19] ($(20 \pm 1)\ R_\odot$), [20] ($(11.8 \pm 1.0)\ R_\odot$), [21] ($(19 \pm 4)\ R_\odot$). The photometric behavior of AU Peg is characterized by noticeable evolutionary changes in the brightness variation period. Based on published data, the change in the pulsation period was traced in detail over the date interval JD2432000–2458000 [19, 22]. During this time, a smooth increase in the period occurred from $P_{\rm pls} \approx 2.388^d$ to $P_{\rm pls} \approx 2.412^d$. It should be noted that any phase mismatch between the light curve and the pulsation curve of radial velocity variations caused by failure to take into account period changes between series of photometric and spectroscopic observations can lead to significant (up to 30%) systematic errors in determining the radius using the pulsating photosphere method [23]. It is also worth noting that assumption [24] that AU Peg is a bimodal Cepheid with a ratio of the periods of the first overtone and the fundamental tone of about 0.706. In our opinion, we are encountering here a rare and surprising case of an almost exact coincidence of the period of the first overtone with one day aliasing period of the fundamental one, i.e., their relationship in the form $P_F^{-1} + P_1^{-1} \approx 1.0$, and for this reason the "traces" of the secondary period noted in [24] are associated with the effect of daily aliasing.

The Gaia eDR3/DR3 catalogues provide values of the trigonometric parallax (*plx* ≈ (1.6463 ± 0.020) mas) and proper motion components *pmRA* ≈ (−2.58 ± 0.02) mas/yr, *pmDE* ≈ (−12.97 ± 0.015) mas/yr [25–27]. Bayesian estimates of the "geometric" and "photogeometric" distances [28] are *rgeo* ≈ (597±7 pc), *rpgeo* ≈ (594 ± 6) pc, respectively. For the galactic longitude $b \approx -22.27°$ we can estimate the present-day z-coordinate of AU Peg: $z \approx -200$ pc. Taking into account all known parameters and the known radial velocity of the system (about −1 km/s; see below and references in the cited papers), we calculated the parameters of the Cepheid galactic orbit in the Besancon Galaxy Model (BGM) [29–32] (the orbit calculations are available at https://gravpot.utinam.cnrs.fr/). The calculations showed that the orbit of AU Peg is enclosed in an orbital torus with a height of $|z| \le 0.3$ kpc and inner and outer radii of 7.2–8.8 kpc in projection onto the galactic plane. The tangential velocity of the system varies within (225–255) km/s, the vertical velocity varies within ±18 km/s, and the period of galactovertical oscillations is about 140 million years. In [33], based on a study of the spatial-age distribution and kinematics of open clusters, it was shown that such an amplitude of vertical velocities and a half-thickness of the orbital torus of the order of 0.3 kpc are characteristic of open clusters with an age of about 1–3 Gyr (see Figs. 8, 13 in the cited work). The well-known phenomenon of secular growth of velocity dispersion [34] allows us to assert that a stellar population with an age of about 3 Gyr is characterized by a vertical velocity dispersion of about 15 km/s, which is close to the observed vertical velocity of the AU Peg system. Based on the shape and kinematic parameters of the orbit, and taking into account a number of spectroscopic estimates of its metallicity in the range [Fe/H] ∼ −0.2...+0.33 [18, 35, 36] and the estimate from the LAMOST DR7 catalog [Fe/H] ≈ +0.165 ± 0.06 [37] (i.e., the chemical composition characteristic of the disk), we can confidently state that the Cepheid AU Peg belongs to the population of the Galactic disk of moderate age and is not an object of the halo or thick disk. This allows us to confidently reject the classification of AU Peg as a BL Her variable.

As it follows from to the Gaia DR3 astrometric data, the true distance modulus of the Cepheid AU Peg is $(m - M)_0 \approx 8.88 \pm 0.02$ mag. Estimates of its color excess are $E(B-V) \le 0.10$ mag [18, 38], $E(B-V) \approx 0.09$ mag [39], and $E(B-V) \approx 0.07 \pm 0.02$ mag (STILISM 3D absorption map [40–43]). All estimates agree well with each other, and their differences lead to variations in the absorption value of no more than $\Delta A_V \le 0.03$–0.05 mag.

2. RADIAL VELOCITIES, PHOTOMETRY, AND ORBITAL PARAMETERS OF AU Peg

2.1. Radial Velocity Samples

The data on the radial velocity measurements used are presented in Table 2. Columns 1–4 contain the series number, number of observations, JD interval, and reference to the data source, respectively. The total number of measurements taken from 7 data sources was 355. Taking into account the noticeable increase in the pulsation period, 3 separate samples with non-overlapping observation dates were com-

Table 2. Sources of data on the radial velocities of the Cepheid AU Peg. The numbers of observation series no., number of observations N, Julian date intervals and references are given

No.	N	JD2400000	Data source
1	173	47739–51092	[4, 5], [6]
2	74	53930–59490	Table 1
3	65	43738–44960	[18]
4	23	44062–44949	[59]
5	20	49957–50009	[60]

piled from 5 series of radial velocity measurements to calculate the orbital parameters. The first sample includes series 1 and 5 in Table 2. 2, the second sample is series 3, 4, and the third is the most recent series of our previously unpublished measurements under number 2. The calculations of the orbital parameters were based on the representation of the measured radial velocity as a contribution from the orbital motion along an elliptical orbit relative to the common center of mass and a pulsation contribution described by a trigonometric series of order $N = 4$:

$$V_{\rm pls}(i) = \sum_{k=1}^{N}\left[A_k \sin\left(2\pi k\frac{t_i - t_0}{P_{\rm pls}}\right) + B_k \cos\left(2\pi k\frac{t_i - t_0}{P_{\rm pls}}\right)\right], \quad (1)$$

where A_k, B_k are the amplitudes of the harmonics (as an example, they are given in Table 3 for the solution obtained from the densest sample, including series number 1 and 5), $P_{\rm pls}$ is the pulsation period, t_i is the time of observations, t_0 is the time chosen for convenience of presenting the pulsation curve so that in phase $\Phi_{\rm pls} = 0$, $V_{\rm pls} = 0$. Note that the value of the pulsation period was determined by spectral methods from series of photometric data (see the next section).

2.2. Quasi-Simultaneous Measurement Series of Brightness and Radial Velocity

To estimate the radius of AU Peg and to determine its evolutionary status, we used the most reliable published photometric data. As already mentioned, the noticeable variability of the Cepheid period requires that the photometric and spectral measurements used be as close as possible in the observation intervals to avoid mismatches in the phases of the brightness and radial velocity variations. We had at our disposal brightness measurements in the (*B, V*) bands taken from [18, 19, 22, 44, 45], a total of more than 220 observations, of which about 150 brightness measurements were used, quasi-simultaneous with the radial velocity measurements. Also used were 44 measurements of brightness in the (*G*, *BP*, *RP*) bands

Table 3. Coefficients of expansion of the pulsation curve for radial velocity series numbers 1 and 5 (initial epoch t_0 = JD2450001.094 and pulsation period $P_{\rm pls} = 2.4112^d$)

Harmonic k	A_k	B_k
1	+11.40648	−0.61652
2	−3.45623	+0.77264
3	+1.30309	−0.20351
4	−0.76163	+0.03757

(JD2456962–2457887) from the Gaia DR3 light curve catalog [25, 27, 46] (VizieR Online Data Catalog I/355/epphot). To determine the orbital parameters and radius from the 1st and 5th rows of radial velocities (JD2447739–2450009), a series of photometric observations was compiled quasi-simultaneously with the spectral data: 23 measurements from [19] (JD2448068–2448594), 40 measurements from [22] (JD2449538–2451080). As a result, the photometric series contains 63 measurements of brightness in the (*B, V*) bands in the interval (JD2448068–2451080). The light curve in this date range is well described by a period of about 2.4112 days. For the 3rd and 4th radial velocity series (JD2443728–2444960), a quasi-simultaneous series of photometric observations was also compiled: 30 measurements from [45] (JD2444071–2444910), 3 measurements from [18] (JD2444089–244491), 39 measurements from [44] (JD2443610–2443809), 15 measurements from [19] (JD2443714–2444870); as a result, the photometric series contains 87 brightness measurements in the (*B, V*) bands (JD2443610–2444910). The photometric period at this epoch was 2.4053 days.

Our previously unpublished radial velocity measurements (series 2, JD2453930–2459490, presented in this paper in Table 1) were, by a happy coincidence, carried out almost simultaneously with the photometric measurements made within the Gaia mission (44 brightness measurements in the bands (*G*, *BP*, *RP*) in the period JD2456962–2457877). To ensure greater synchronicity, we decided to use only 53 radial velocity measurements in the date interval JD2455492–2459490. The pulsation period is 2.4125 days.

2.3. Determination of the Orbital Parameters of AU Peg

Determination of the orbital parameters was based on the well-known description of the motion of the binary system components along elliptical orbits. To reduce the time of parameter calculations, we used a technique of dividing all the parameters to be determined into "nonlinear" and "linear" ones, described in [47]. The "nonlinear" unknowns include the moment of passage through the pericenter of the orbit

Table 4. AU Peg orbit parameters

Parameters	Variants		
	series 1 + 5	series 3 + 4	series 2
JD−2400000	49554−50009	43738−44960	55492−59490
P_{pls}, days	2.4112	2.4053	2.4125
T_0−2400000	—	50004.34 ± 6.78	50090.90 ± 3.56
P_{orb}, days	53.331 ± 0.008	53.370 ± 0.033	53.331 ± 0.004
e	0.014 ± 0.007	0.120 ± 0.021	0.026 ± 0.010
Ω, rad	0.007 ± 0.460	6.23 ± 0.19	6.26 ± 0.42
K, km/s	46.01 ± 0.29	42.19 ± 0.89	44.88 ± 0.46
V_γ, km/s	−1.62 ± 0.25	−2.54 ± 0.67	−0.68 ± 0.35
$f(M)$, $M_\odot$	0.539 ± 0.010	0.407 ± 0.026	0.520 ± 0.016
$a_1 \sin i$, a.u.	0.226 ± 0.002	0.206 ± 0.004	0.220 ± 0.002
RMS, km/s	2.62	4.02	1.97

T_0, the orbital period P_{orb}, the eccentricity e and the longitude of the ascending node Ω. All other problem parameters, such as the amplitude of the orbital velocity K, the velocity of the center of mass V_γ and the coefficients of the trigonometric expansion of the pulsation contribution (A_i, B_i) are included in the problem linearly. The results of the orbit calculations and their errors for the three above-mentioned samples of radial velocities are given in Table 4: T_0 is the moment of orbital pericenter passage; P_{orb} is the found value of the orbital period; e is the orbital eccentricity; Ω is the longitude of the ascending node; K is the amplitude of the orbital radial velocity variation; V_γ is the radial velocity of the system's center of mass; $f(M)$ is the mass function; $a_1 \sin i$ is the projection of the semi-major axis of the primary component's orbit onto the line of sight. Each variant was calculated with its own value of the pulsation period P_{pls}, which best describes the brightness and radial velocity variations; their values are given in the second row of the table. The last row of the table gives the root-mean-square deviation from the general solution for each calculation variant. The smallest scatter is shown by the series of the most recent measurements under number 2. We believe that the radial velocity measurements were carried out during a period of a certain "stabilization" of P_{pls} after a long period of its monotonic growth (see, for example, Fig. 7 in [22]), while the pulsation contributions to the remaining series are much worse described by a single period value.

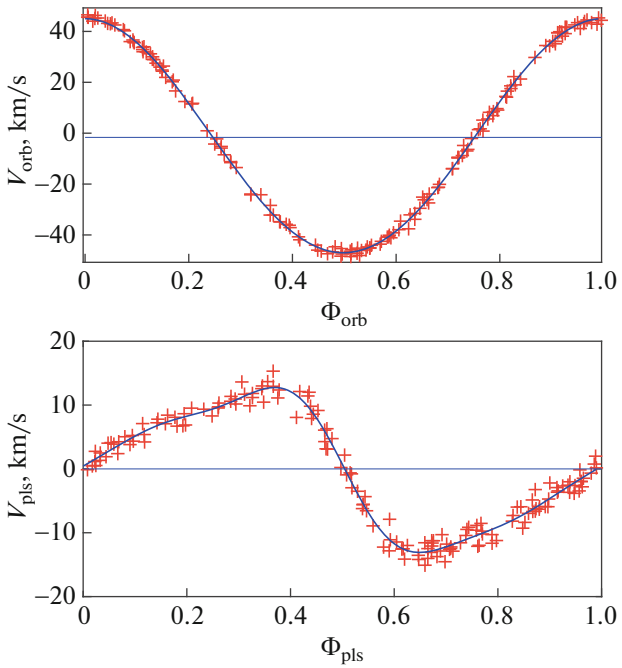

Fig. 1. Example of separating the orbital (top) and pulsational (bottom) contributions to the radial velocity for the solution obtained from observation series 1 and 5. Φ_{orb} and Φ_{pls} are the orbital and pulsational phases, respectively. The pulsational contribution was represented by a fourth-order trigonometric series (see (1) and Table 3). The horizontal line in the upper panel is the systemic velocity level V_γ. The solid blue lines are the approximation. The red crosses show individual measurements (the residual deviation from the model velocity was equally divided between the orbital and pulsational contributions).

An example of the decomposition of the radial velocity into the contributions of orbital motion and pulsations for the largest sample, including 193 radial velocity measurements (series 1 and 5), is shown in Fig. 1. The extracted radial velocity curves were used to estimate the pulsation radius of AU Peg using a modified method [48] with expansion in color index up to 2–3 orders [23].

2.4. Estimates of the Pulsational Radius of AU Peg

In our previous work [47], to determine the pulsational radius of the Cepheid V350 Sgr, we used the previously developed so-called "thermal" method [49], which is based on modeling multiphase variations in $T_{\rm eff}$ using the color calibration of the effective temperature that we derived for classical Cepheids. However, in this case, we are not completely sure that this calibration is applicable to the unusual Cepheid AU Peg. Therefore, to estimate the radius variations, we used a generalization of the method [48], which consists in representing the observed light curve in a general form suitable for any pair of photometric bands:

$$Magn = -5\log[\langle R\rangle + r(t)] + \sum_{k=1}^{K} a_k CI^k + C,$$

where *Magn* is the apparent brightness of the star, *CI* is the observed color index, (a_k), *C* are the constant coefficients, $\langle R\rangle$ is the average radius, $r(t)$ is its change with phase. A significant advantage of this method compared to the surface brightness method [50] is the fact that the mean radius is determined using uncorrected for extinction brightness variation curves and color indices [23]. As shown in [51], all the information about the extinction in expression (2) is included in the constant *C*. As usual, the radius variations $r(t)$ are calculated by integrating the pulsation radial velocity curve taking into account the projection factor (see the discussion of the problem in [47]). We used a series of values of the projection factor *PF* in the range 1.28–1.34, leading to practically identical values of the mean radius within the error limits. Note that AU Peg is distinguished by a very small amplitude of brightness and color variations (about 0.3–0.4 mag), therefore the relative accuracy of the photometric measurements plays a decisive role in determining the mean radius. The analysis showed that the greatest scattering of the light curves and color indices is in the photometric series quasi-simultaneous with series 1 and 5 of radial velocities (63 (*B, V*) measurements taken from two sources); this is precisely why it leads to a value of the mean radius $\langle R\rangle/R_\odot \approx 10 \pm 1$, which differs sharply from the solution for series 3 and 4 of radial velocities (87 (*B*, *V*) measurements from four sources) ($\langle R\rangle/R_\odot \approx 16.0 \pm 1.1$) and series 2 ($\langle R\rangle/R_\odot \approx 16.0 \pm 0.6$) (44 measurements of Gaia DR3 in the (*G*, *BP*, *RP*) bands). Obviously, the most reliable results can be obtained using our previously unpublished radial velocity measurements (series 2) together with Gaia DR3 photometric observations, the declared relative flux accuracy of which is ±0.001 (which is equivalent to a brightness measurement accuracy of about ±0.001 mag). It should also be noted that the Gaia observations are not burdened by period aliasing effects, which simplifies the analysis of periodicities. The results of calculating the mean radius of AU Peg and the radius variations from Gaia DR3 photometry for the light and color curves (*RP, BP–RP*) using our new radial velocity measurements (series 2) are shown in Fig. 2. The mean radius of a Cepheid is one of the most important astrophysical parameters, carrying independent information about its evolutionary status. Note that the obtained estimate of the mean radius is preliminary, since its calculation used photometric data not corrected for the contribution of the satellite.

3. ELLIPSOIDALITY EFFECT AND RESTRICTIONS ON THE MASSES OF THE MAIN COMPONENT OF AU Peg AND THE COMPANION

When analyzing photometric data in the Gaia DR3 *G* band, we managed to detect for the first time for spectroscopic binary Cepheids nearly sinusoidal brightness variations of AU Peg with a half-orbital period of 26.6653 days at a level of $\Delta G \approx 0.02$ mag (which roughly corresponds to a relative flux change of 2%) (they are shown at the bottom left in Fig. 3). Taking into account the short orbital period of the AU Peg system and the presence of a more massive companion, as well as the previously expressed suspicions about the partial filling of the Roche sphere by the Cepheid [17, 35], we can confidently interpret the brightness variations we discovered as a manifestation of the effect of the ellipsoidality of the primary component. Even greater confidence in this conclusion is given by the clear consistency of the brightness variations with the phases of the orbital motion: the brightness of AU Peg in the quadrature phases (i.e., at maximum radial velocity values) is systematically higher than in the phases of conjunction (near the zero velocity value). In quadratures, the lateral surface of the prolate spheroid of the star is projected onto the celestial sphere, and in conjunctions, its frontal section. Obviously, the manifestation of the ellipsoidal effect associated with the tidal interaction of the Cepheid and its companion imposes additional restrictions on the ratio of the component masses and the angle of inclination of the relative orbit to the plane of the sky and allows us to somewhat clarify the evolutionary status of the system.

Figure 4 shows a number of diagnostic diagrams constructed for the value of the average radius of the Cepheid $\langle R\rangle/R_\odot \approx 16$ and allowing us to clarify the masses of the Cepheid and companion and the orientation of the orbit of the system. To construct the diagrams, we used well-known methods for analyzing the ellipsoidal effect, exhaustively described in the monograph [52]. All diagrams are constructed in the form of dependences of the parameters on the Cepheid mass $M_1/M_\odot$. In order not to clutter the diagrams, a series of values of the inclination angles of the relative orbit of the system $i = (52, 54, 60, 65, 70, 75)°$ were selected. Using the value of the mass function taken from

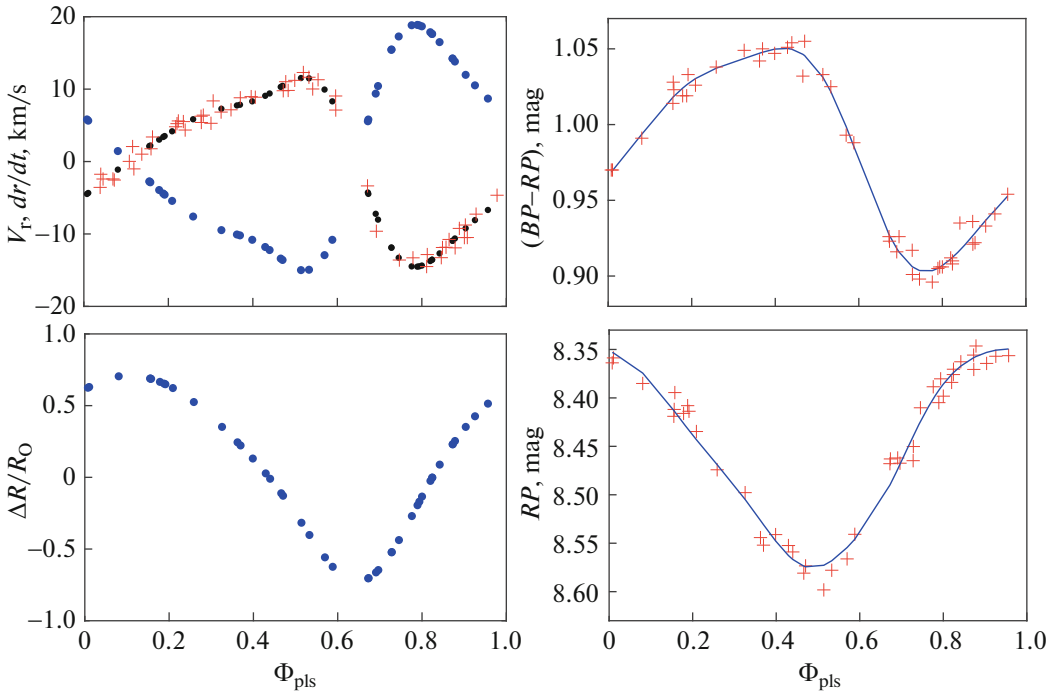

Fig. 2. Variations in the AU Peg radius calculated by the generalized method [48] from Gaia DR3 photometry data in the (*RP*, *BP*−*RP*) bands using our radial velocity measurements (series 2). Right: Color index curve (*BP*−*RP*) (top) and *RP* light curve (bottom). Red crosses are observations, blue line is the result of smoothing using a trigonometric series. Left: radial velocity V_r (red crosses) and photospheric pulsation velocity dr/dt (blue dots) for $PF = 1.30$ (top). Curve of radius variations (in solar radii) (bottom, blue dots). The average radius is $\langle R\rangle/R_\odot \approx 16.0 \pm 0.6$.

Table 4, the relationships between the masses of the Cepheid and the companion ($M_2/M_\odot$) were calculated for each of the inclination angles, shown in the upper left corner of Fig. 4. The lower black dashed line limits the eclipse region from above for the mass of the companion M_2 under the assumption that the companion is a main-sequence star (the "mass–radius" relationship is taken from [53]). It is clearly seen that in fact, inclination angles $i > 75°$ can be excluded from consideration. The upper black dashed line (and the dashed line in the upper middle figure for the mass ratio M_1/M_2) constrain the variants with the mass of the companion $M_2/M_\odot \geq 2.0$, for which the hot companion (A1V–A2V or earlier spectral class) should have made a significant contribution to the brightness of the system in the short-wavelength bands (*B, BP*), while the system is characterized by red color indices $\langle(B-V)\rangle_0 \approx 0.77$ mag, $\langle(BP-RP)\rangle_0 \approx 0.87$ mag, and taking into account the contribution of the hot companion will lead to a noticeable increase in the normal color indices.

We will try to justify this choice by estimating the contributions of the A1V–A2V companion and the Cepheid itself to the total brightness of the AU Peg system in the Gaia DR3 bands (*BP*, *RP*) and (*B*, *V*). From the very reliable Bayesian distance estimates [28] of the order of $D \approx 594$–597 pc, the true distance modulus is derived: $(m - M_0) \approx 8.88 \pm 0.02$ mag. The average values of the AU Peg system are $\langle BP\rangle \approx 9.45$ mag and $\langle RP\rangle \approx 8.48$ mag. For the color excess $E(B-V) \approx 0.08$ mag and the absorption $A_V \approx 0.25$ mag, the absorption in the Gaia DR3 bands can be estimated: $A_{BP} \approx 0.25$ mag, $A_{RP} \approx 0.15$ mag [54]. Therefore, the absorption-corrected magnitudes of the system in the Gaia DR3 bands are $\langle BP\rangle_0$(tot) ≈ 9.20 mag and $\langle RP\rangle_0$(tot) ≈ 8.33 mag, and then the absolute magnitudes are $\langle M_{BP}\rangle$(tot) $\approx +0.32$ mag and $\langle M_{RP}\rangle$(tot) ≈ -0.55 mag. In the (*B*, *V*) bands, the average apparent brightness of the system is $\langle B\rangle_0$(tot) ≈ 10.10 mag, $\langle V\rangle_0$(tot) ≈ 9.25 mag, and the absolute magnitudes are $\langle M_B\rangle$(tot) $\approx +0.89$ mag and $\langle M_V\rangle$(tot) $\approx +0.12$ mag, respectively. From the calibration of the luminosity of dwarf stars [55], we find for the companion of spectral type A1V–A2V $\langle M_{BP}\rangle$(sat) $\approx +1.37$ mag, $\langle M_{RP}\rangle$(sat) $\approx +1.30$ mag, $\langle M_B\rangle$(sat) $\approx +1.42$ mag and $\langle M_V\rangle$(sat) $\approx +1.35$ mag. From these data, it is easy to estimate the contribution of the massive companion to the total mean fluxes in the (*BP, RP*) (~38%, ~18%) and (*B*, *V*) (~32%, ~61%) bands, which seems to be quite significant; obviously, at minimum brightness the contribution of the companion is even greater. Taking into account the contribution of the companion leads to the following approximate estimates of the absolute magnitude of the primary component:

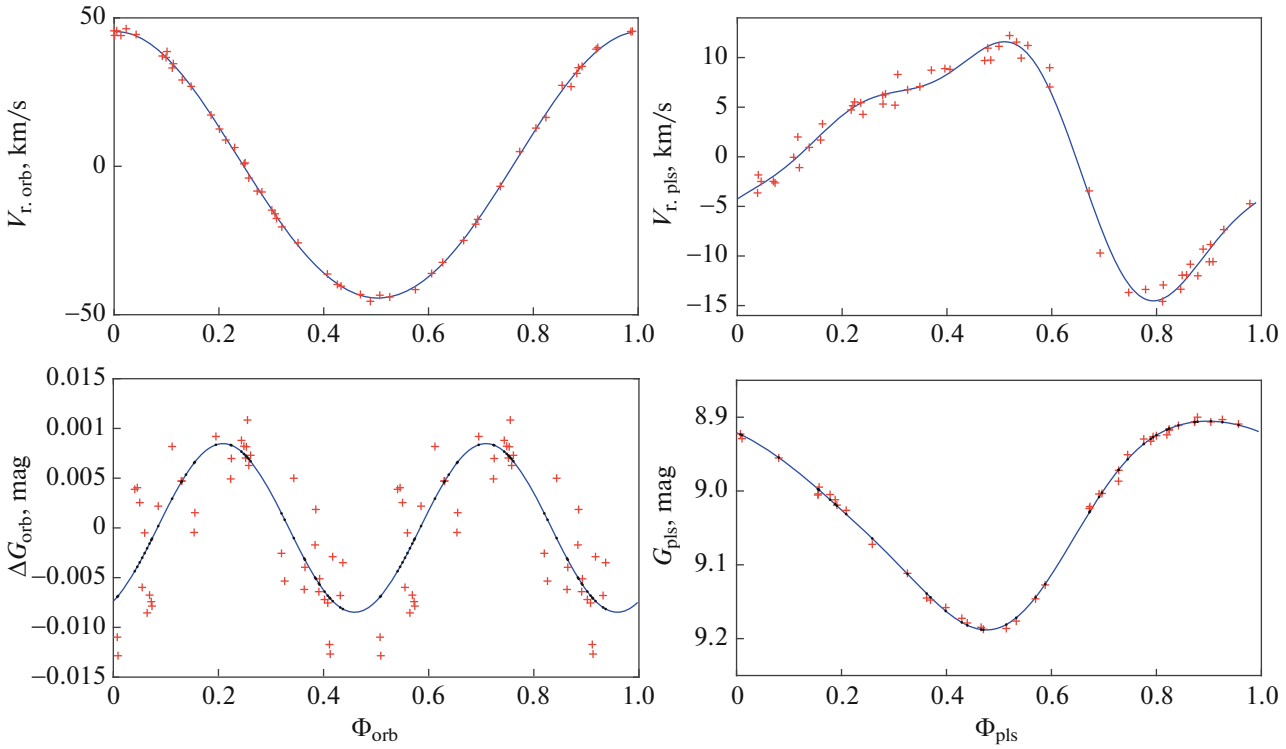

Fig. 3. Top: Decomposition of the AU Peg radial velocity into orbital motion (left) and pulsation (right) contributions for series 2 radial velocities (JD2455492−2459490). Bottom: Decomposition of the G-band light curve from Gaia DR3 data. On the left are the brightness variations due to the ellipsoidal effect at a level of ±0.01 mag with a period equal to half the orbital period (26.6653 days). On the right is the *G*-band light curve (pulsation period $P_{pls} = 2.4125374$ days). The phases are counted from the moment $T_0 = \text{JD}2450090.895$.

$\langle M_{BP}\rangle$(AU Peg) ≈ +0.84 mag and $\langle M_{RP}\rangle$(AU Peg) ≈ −0.33 mag, and the normal color index of the primary component increases to at least $\langle BP{-}RP\rangle_0 \approx 1.17$ mag. Such a color index is more typical for a star with $T_{\rm eff} \lesssim$ 5000 K, while for AU Peg in different pulsation phases, spectroscopic estimates from $T_{\rm eff} \sim$ 5300 K [18, 37] to $T_{\rm eff} \sim$ 5750 K [21, 35] and $T_{\rm eff} \sim$ 6000 K [36] were derived. It follows that the limit on the satellite mass $M_2(\max)/M_\odot \sim 2.0$ seems to be, most likely, too high.

In the lower left figure, using the tabulated value of $a_1 \sin i$ and the mass ratios, a family of mutual distances of the components $A/R_\odot$ is calculated. To estimate the radius of the Roche sphere $R_L/R_\odot$ of the Cepheid as a function of the mass ratio and the distance between the components, we used formula (2) derived in [56], which gives an approximation for the relative radius of the Roche sphere with an accuracy of about 1%. The family of absolute sizes of the Roche surfaces (expressed in $R_\odot$) is shown in the lower middle figure. The upper right figure shows the degree of filling of the Roche sphere R_1/R_L by the star as a function of the mass of the primary component of the system. To estimate the magnitude of the ellipsoidality effect (its contribution to the total flux), we used the approximation for the star's shape as a prolate spheroid and the expressions for the projections of the spheroid onto the plane of the sky derived in [57] for this simple case, also published in the monograph [52] (formulas (234)–(235), p. 97). The corresponding family of curves for the dependence of the ellipsoidality contribution on the mass of the primary component for a number of values of the orbital inclination angle i is shown in the lower right panel of Fig. 4, where the black horizontal line denotes the observed magnitude of the ellipsoidality effect. This diagnostic diagram allows us to fairly confidently estimate the possible upper limit on the mass of AU Peg based on the coordinate of the intersection of the red curve, constructed for the inclination angle $i \approx 75°$, with the line $\Delta G \approx 0.02$ mag. Taking into account that the calculated families of curves depend on the adopted value of the Cepheid radius $\langle R\rangle/R_\odot$, and the error in determining the radius is approximately 0.6 $R_\odot$, we estimate the probable upper limit of the Cepheid mass at $M_1(\max)/M_\odot \approx 0.85 \pm 0.05$.

From the presented diagnostic diagrams, it is easy to see that the minimum mass of the companion should be $M_2(\min)/M_\odot \approx 1.50 \pm 0.05$. Note also that taking into account the contribution of the companion

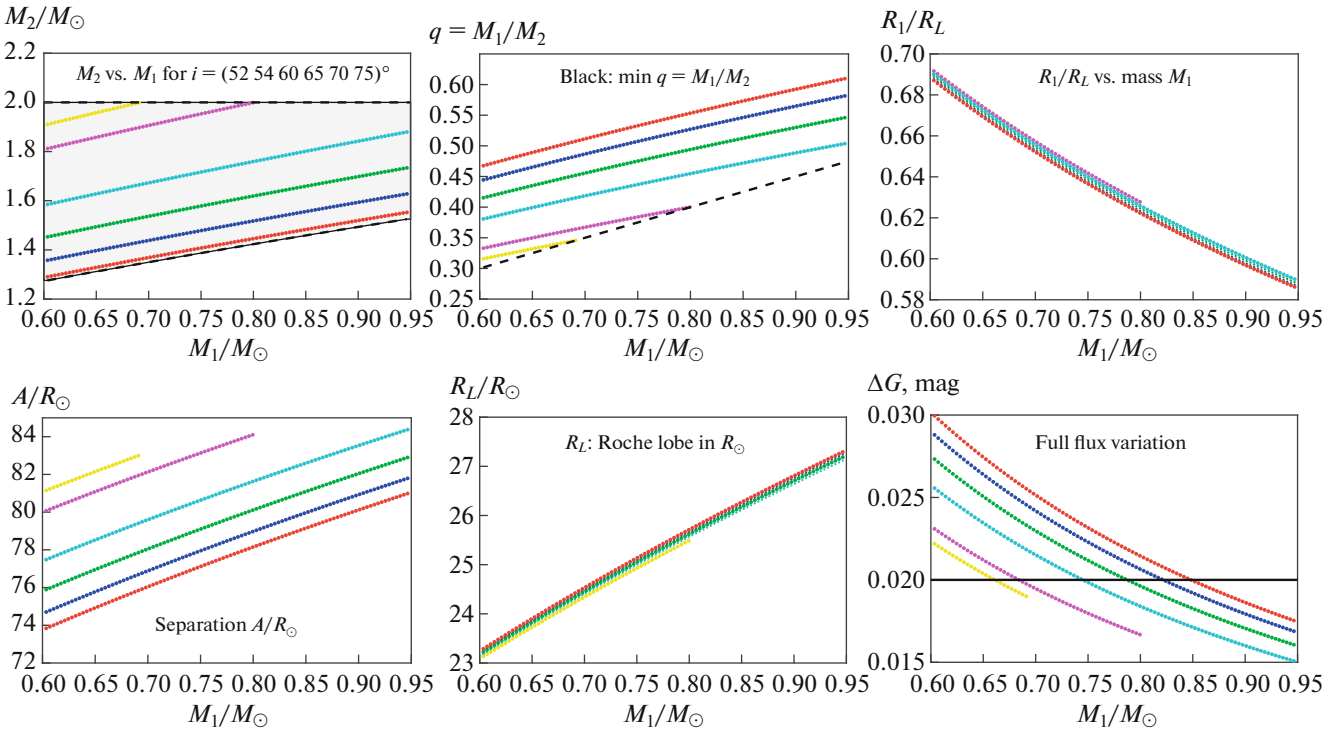

Fig. 4. Diagnostic diagrams for AU Peg. Dependences of the parameters—the mass of the companion, mass ratio M_1/M_2, radius of the Roche sphere $R_L/R_\odot$, degree of filling of the Roche sphere, distance between the components $A/R_\odot$, ellipsoidal effect ΔG—on the mass of the primary component for a set of orbital plane inclination angles i = (52, 54, 60, 65, 70, 75)°. The lower black dashed line in the upper left figure limits the "forbidden zone" in which mutual eclipses of the components are possible. The "allowed" inclination angles $i \le 75°$. The upper dashed line in this diagram corresponds to the maximum mass of the companion, at which it makes a decisive contribution to the total brightness of the system. The black solid line in the lower right figure denotes the observed level of variability due to the ellipsoidal effect, $\Delta G \approx 0.02$ mag. Details are discussed in the text.

to the integral brightness of the system will lead to some increase in the relative flux variation ΔG caused by the ellipsoidality of the main component and, in turn, to a decrease in the upper limit of its mass.

The lower limit of the Cepheid mass is estimated less confident. It can be estimated from the coordinate of the intersection of the line $\Delta G \approx 0.02$ mag with the yellow curve in the lower right diagram (constructed for an inclination angle of $i \approx 52°$). With allowance for the error in estimating the mean radius, it can be considered equal to $M_1(\min)/M_\odot \approx 0.65 \pm 0.05$ with an upper limit on the mass of the companion of about $M_2(\max)/M_\odot \approx 1.95$. Taking into account what was said above about the significant contribution of the more massive companion to the total brightness, as a first approximation, we have the right to consider the indicated lower estimate of the Cepheid mass to be quite plausible. At the same time, the range of possible values of the orbital inclination angle narrows to ~50°–75°.

For the given range of Cepheid mass values, the degree of filling of the Roche sphere can be 60–70%.

Table 5 presents the estimates of the mass of the companion $M_2/M_\odot$, the distance between the components $A/R_\odot$, the radius of the Roche sphere $R_L/R_\odot$ $R_\odot$, and also (except for $M_1/M_\odot \approx 0.65$) the average absolute magnitudes of the primary component of the AU Peg system for different assumptions on the mass of the primary component $M_1/M_\odot \approx 0.85$, 0.80, 0.75, 0.70, 0.65 after subtracting the contribution of the companion to the Gaia DR3 bands (*BP*, *RP*) and the bands (*B*, *V*) are given. Approximate values of the orbital inclination angle are also given for each of the variants, which for a given combination of masses $M_1/M_\odot$ and $M_2/M_\odot$ satisfy the constraint ($\Delta G \approx$ 0.02 mag) on the magnitude of the ellipsoidality effect. Obviously, taking into account the contribution of the hotter companion leads to an increase in the normal color indices $\langle B-V\rangle_0$ from 0.77 mag to 0.82–0.94 mag, and the color indices $\langle BP-RP\rangle_0$ from 0.87 mag to 0.93–0.98 mag. As an example, Fig. 5 shows a comparison of the original and corrected light curves and the color index in the bands (*RP*, *BP*) with allowance for the minimum photometric contribution corresponding to a companion with a mass of

Table 5. Estimates of the masses of AU Peg $M_1/M_\odot$ and the companion $M_2/M_\odot$, distance between the components $A/R_\odot$, radius of the Roche sphere $R_L/R_\odot$, mean absolute magnitudes of the primary component of the system corrected for the contribution of the companion, and the orbital inclination angles (calibrations from [55] were used). For the primary component with $M_1/M_\odot \sim 0.65$, the contribution of the massive companion to the total brightness of the system is too large and estimates are not given

$M_1/M_\odot$	$M_2/M_\odot$	$A/R_\odot$	$R_L/R_\odot$	$\langle M_{BP}\rangle$, mag	$\langle M_{RP}\rangle$, mag	$\langle M_B\rangle$, mag	$\langle M_V\rangle$, mag	i, deg
0.85	~1.50	~79.0	~26.2	+0.43	−0.48	+1.04	+0.22	~75
0.80	~1.57	~79.5	~25.7	+0.45	−0.47	+1.08	+0.24	~67
0.75	~1.70	~80.7	~25.2	+0.47	−0.46	+1.12	+0.26	~60
0.70	~1.85	~81.0	~24.5	+0.55	−0.43	+1.25	+0.31	~55
0.65	~2.0	~83.0	~23.7	—	—	—	—	~52

$M_2/M_\odot \approx 1.50$ in the pulsation cycle. It is easy to understand that for masses $M_1/M_\odot \le 0.85$ of the primary system component, the differences between the original and corrected curves will be even more significant. Strictly speaking, photometric correction should be performed before calculating the pulsation radii of the Cepheid, since the calculation results depend significantly on the shape of the light and color curves. Therefore, the previously noted value of the Cepheid radius, equal to 16 $R_\odot$, should be considered as a first approximation. Then, in the second approximation, we used the corrected photometry data to refine the radius variations at masses $M_1/M_\odot =$ 0.80, 0.75. The estimates of the average Cepheid radius increase to approximately 16.7 $R_\odot$. An increase in the Cepheid radius, in turn, will lead to a small increase in all M_1 estimates by approximately 0.05 $M_\odot$, which is practically within the declared errors; and the increase in the M_1 estimates will be accompanied by a slight decrease in the M_2 mass and the contribution of the companion to the photometric fluxes. The relative stability of the radius estimates is due to the nearly symmetric shape of the light curve and the small amplitude of the brightness and color changes.

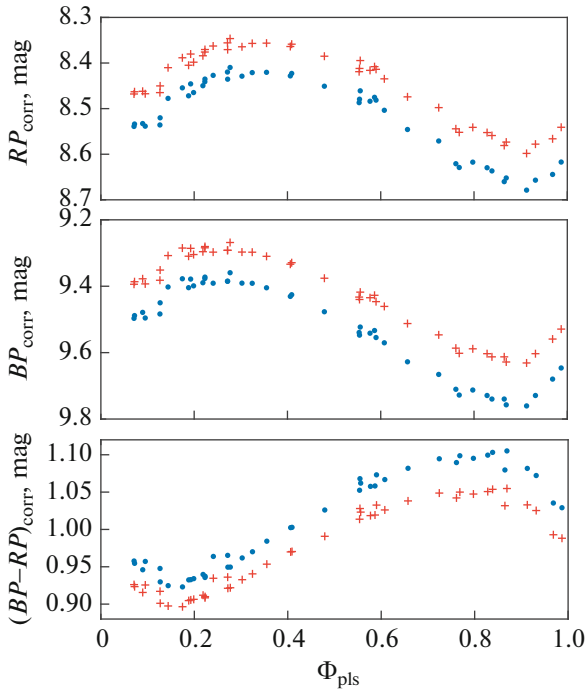

Fig. 5. Example of correction of Gaia DR3 photometric data uncorrected for interstellar extinction and reddening due to for the contribution of a companion with a mass of $M_2/M_\odot \approx 1.50$. Red crosses are the original data, blue dots are the corrected light and color curves. From top to bottom: band light curves (*RP*, *BP*) and color index curve (*BP*–*RP*).

4. EVOLUTIONARY AND PULSATIONAL STATUSES OF THE AU Peg SYSTEM

Based on the estimates of the mass of the main component of the system in the range of (0.60–0.85) $M_\odot$ and the estimates of the radius of the order of (15.5–16.5) $R_\odot$, we can estimate the value of $\log g \sim$ 1.8–2.0 in good agreement with the spectroscopic estimates [36, 38]. The mass estimates we derived lead to a mass ratio of $1.7 \lesssim M_2/M_1 \lesssim 3$. Some time ago, a mass exchange undoubtedly occurred in the system, as a result of which the more massive component, having lost a significant part of its mass, became a subgiant with a mass less than ~0.85–0.9 $M_\odot$.

The present-day sum of the masses of the components is (2.4–2.6) $M_\odot$, as follows from our results. It is possible that some part of the envelope mass was lost in the flow of matter, and it is possible that the mass loss is still ongoing: the literature contains estimates of the mass loss rate ranging from 10^{-6} $M_\odot$/year [17] to 4×10^{-4} $M_\odot$/year [16]. This is supported by the IR excess of the system, which is generally characteristic of Cepheids [17], and the estimate of the temperature of the gas-dust component reaches ~500 K. Therefore, the initial mass of the main component of the system could not have been less than half of the cur-

rent total mass of the system, i.e., $\sim(1.2-1.3)\ M_\odot$. The MESA evolutionary tracks [58] for [Fe/H] $\sim +0.1$ dex predict the evolution time of stars with initial masses (1.2, 1.3) $M_\odot$ from the main sequence to the red giant branch, where mass exchange can begin, to be about ~6 and ~5 Gyr, respectively. To reconcile the estimates of the evolutionary and "kinematic" ages of (~1–3) Gyr, it should be assumed that the initial mass of the main component of the AU Peg system must have been at least ~1.5 $M_\odot$, for which the evolution time to the red giant stage is about 3 Gyr. However, this argument can hardly be considered decisive, since the Sun, with a sufficiently large evolutionary age, has a position in the Galaxy and kinematics characteristic of young disk populations. Nevertheless, taking into account the possible loss of the total mass of the system, the estimate of the initial mass of the main component of about ~1.5 $M_\odot$ seems quite plausible. In this case, the main component should have lost at least (0.6–0.7) $M_\odot$ during the mass exchange, and the companion should have increased its mass to at least $M_2(\mathrm{min}) \sim 1.5\ M_\odot$. Within the framework of such a very rough scenario, the initial mass of the companion could have been about ~1 $M_\odot$.

In [18], it was shown that AU Peg is located beyond the red boundary of the instability strip for BL Her variables (see Fig. 4 in the cited article). If we take into account that due to the overestimated distance (more than 1 kpc) adopted in the paper cited and the non-accounting the contribution of the companion to the integral brightness of the system, the luminosity of the main component was greatly overestimated, the conclusion about the position of the Cepheid relative to the instability strip only strengthens. Recently, the authors of [14, 15] performed calculations of pulsations in the linear and nonlinear approximations for a grid of models of BL Her-type variables in a wide range of masses (0.5–0.8) $M_\odot$, abundances of heavy elements $Z \sim$ (0.001–0.013), effective temperatures $T_{\mathrm{eff}} \sim$ (5300–6800) K, radii $R/R_\odot \sim$ (6–20), bolometric luminosities $M_{\mathrm{bol}} \sim$ (−1.40...+0.35) mag and pulsation periods from 1 to 6 days. Despite the fact that the specified ranges also include the physical parameters of AU Peg, no pulsating model has been found that would simultaneously have a radius of ~16 $R_\odot$, a nearly solar chemical composition with $Z \sim 0.013$, a pulsation period of about 2.4 days, and a luminosity of $L_{\mathrm{bol}} \le 100 L_{\mathrm{bol}}^{\odot}$). Judging by Fig. 1 in [14], in this case AU Peg also lies beyond the red boundary of the instability strip of the calculated models, being an insufficiently hot and bright object. However, taking into account the large uncertainty in the calculations of the position of the red boundary of the instability strip, as well as the detected effects of the gravitational influence of the companion, we could assume that it is the interaction with the companion under conditions of filling the Roche lobe by 60–70% that could excite the proper oscillations of the star in this binary system. Thus, the classification of the very unusual Cepheid AU Peg as a pulsating variable star remains unclear and requires further study from both the evolutionary and pulsation theory points of view. After a single mass exchange, the star is probably still in the stage of evolution from the main sequence to the subgiant branch and most likely gravitational compression and layered hydrogen "burning" serve as its energy source. From an evolutionary point of view, this stage does not correspond to either classical Cepheids or T2 Cepheids, including BL Her variables.

5. CONCLUSIONS

The physical characteristics and evolutionary status of the spectroscopic binary Cepheid AU Peg, previously classified as a T2 Cepheid of the BL Her subclass, have been revised. Based on 74 previously unpublished radial velocity measurements, virtually simultaneous with the astrometric and photometric measurements of the Gaia mission, the parameters of the relative orbit of the Cepheid and its companion have been refined. Using 44 brightness measurements in the (*G*, *BP*, *RP*) bands, variations in the pulsation radius with an amplitude of about 0.7 $R_\odot$ and an average value of $\langle R \rangle \sim (16.0 \pm 0.6)\ R_\odot$ were determined.

Based on the photometric measurements of Gaia DR3 in the *G* band, the relative accuracy of which exceeds 0.1%, the effect of ellipsoidality of the primary component of the AU Peg system was discovered for the first time for binary Cepheids. This effect is expressed in brightness variations at a level of 2% with a half orbital period, and the phases of maximum and minimum brightness are clearly synchronized with the phases of quadratures and conjunctions in the orbital motion, respectively. The observed level of brightness variations allows us to impose fairly stringent additional constraints on the masses of the primary component and the companion, as well as to estimate the degree of filling of the Roche lobe of the primary component at 60–70%. According to the presented estimates, the range of inclination angles of the relative orbit is ~50°–75°, and the corresponding range of possible masses of the primary component is from $\sim(0.85 \pm 0.05)\ M_\odot$ to $\sim(0.60 \pm 0.05)\ M_\odot$. The mass of the companion, calculated from the mass function and the level of variations caused by the ellipsoidality effect, varies within the range from ~1.5 $M_\odot$ to ~2 $M_\odot$, respectively, with the upper limit restricted, in particular, by the contribution of the massive bright companion, a main-sequence star, to the integrated brightness of the system. Obviously, the system experienced mass exchange in the past, and the primary component is currently at the subgiant stage. The orbit of the AU Peg binary system calculated on the basis of astrometric data from Gaia DR3 and radial velocities

is bounded by a torus of thickness $|z| \leq 300$ pc with inner and outer radii of 7.2 and 8.8 kpc, while the vertical velocity lies within $|V_z| \leq 18$ km/s. The position in the Galactic disk and the kinematics characteristic of a thin disk population of moderate age (~1–3 Gyr) completely exclude the classification of AU Peg as a BL Her variable. Taking into account the contribution of the more massive companion to the integrated brightness and color of the system confirms the position of the main component of AU Peg beyond the red boundary of the instability strip. It is also shown that modern pulsation calculations performed for low-mass stars can not explain the causes of the pulsation variability of this unusual object.

ACKNOWLEDGMENTS

The authors are grateful to the participants of the long-term radial velocity measurement program: N.N. Samus, M.E. Sachkov (INASAN), E.V. Glushkova (MSU), A.A. Fedorova (IKI RAS), I.M. Uglova. The authors express their gratitude to A.M. Cherepashchuk and K.A. Postnov for useful consultations on the physics of close binary stars. The study was conducted under the state assignment of Lomonosov Moscow State University. This work used data from the European Space Agency (ESA) mission *Gaia* (https://www.cosmos.esa.int/gaia), processed by the *Gaia* Data Processing and Analysis Consortium (DPAC, https://www.cosmos.esa.int/web/gaia/dpac/consortium). Funding for the DPAC was provided by national institutions, in particular the institutions participating in the *Gaia* Multilateral Agreement.

FUNDING

This work was supported by ongoing institutional funding. No additional grants to carry out or direct this particular research were obtained.

CONFLICT OF INTEREST

The authors of this work declare that they have no conflicts of interest.

REFERENCES

1. N. R. Evans, L. Berdnikov, N. Gorynya, A. Rastorguev, and J. Eaton, Astron. J. **142**, 87 (2011).
2. N. R. Evans, C. Proffitt, K. G. Carpenter, E. M. Winston, G. V. Kober, H. M. Günther, N. Gorynya, A. Rastorguev, and L. Inno, Astrophys. J. **866**, 30 (2018); arXiv: 1808.10472.
3. A. A. Tokovinin, Sov. Astron. **31**, 98 (1987).
4. N. A. Gorynya, T. R. Irsmambetova, A. S. Rastorgouev, and N. N. Samus, Sov. Astron. Lett. **18**, 316 (1992).
5. N. A. Gorynya, N. N. Samus', A. S. Rastorguev, and M. E. Sachkov, Astron. Lett. **22**, 175 (1996).
6. N. A. Gorynya, N. N. Samus', M. E. Sachkov, A. S. Rastorguev, E. V. Glushkova, and S. V. Antipin, Astron. Lett. **24**, 815 (1998).
7. C. Hoffmeister, Astron. Nachr. **240**, 193 (1930).
8. O. J. Eggen, S. C. B. Gascoigne, and E. J. Burr, Mon. Not. R. Astron. Soc. **117**, 406 (1957).
9. I. Soszyński, A. Udalski, M. K. Szymański, Ł. Wyrzykowski, K. Ulaczyk, R. Poleski, P. Pietrukowicz, S. Kozłowski, D. M. Skowron, J. Skowron, et al., Acta Astron. **67**, 103 (2017); arXiv: 1706.09452.
10. I. Soszyński, A. Udalski, M. K. Szymański, Ł. Wyrzykowski, K. Ulaczyk, R. Poleski, P. Pietrukowicz, S. Kozłowski, D. M. Skowron, J. Skowron, et al., Acta Astron. **67**, 297 (2017); arXiv: 1712.01307.
11. I. Soszyński, A. Udalski, M. K. Szymański, Ł. Wyrzykowski, K. Ulaczyk, R. Poleski, P. Pietrukowicz, S. Kozłowski, D. Skowron, J. Skowron, et al., Acta Astron. **68**, 89 (2018); arXiv: 1807.00008.
12. A. Udalski, M. K. Szymański, and G. Szymański, Acta Astron. **65**, 1 (2015); arXiv: 1504.05966.
13. M. Marconi and M. Di Criscienzo, Astron. Astrophys. **467**, 223 (2007); astro-ph/0701256.
14. S. Das, S. M. Kanbur, R. Smolec, A. Bhardwaj, H. P. Singh, and M. Rejkuba, Mon. Not. R. Astron. Soc. **501**, 875 (2021); arXiv: 2011.11626.
15. S. Das, L. Molnár, S. M. Kanbur, M. Joyce, A. Bhardwaj, H. P. Singh, M. Marconi, V. Ripepi, and R. Smolec, Astron. Astrophys. **684**, A170 (2024); arXiv: 2401.11869.
16. H. Harris, E. W. Olszewski, and G. Wallerstein, Astron. J. **84**, 1598 (1979).
17. C. W. McAlary and D. L. Welch, Astron. J. **91**, 1209 (1986).
18. H. C. Harris, E. W. Olszewski, and G. Wallerstein, Astron. J. **89**, 119 (1984).
19. J. Vinko, L. Szabados, and K. Szatmary, Astron. Astrophys. **279**, 410 (1993).
20. C. D. Laney, in *Astrophysical Applications of Stellar Pulsation, Proceedings of the IAU Colloq. 155,* Ed. by R. S. Stobie and P. A. Whitelock, ASP Conf. Ser. **83**, 367 (1995).
21. Z. Balog, J. Vinko, and G. Kaszas, Astron. J. **113**, 1833 (1997).
22. G. Csörnyei and L. Szabados, Astrophys. Space. Sci. **364**, 151 (2019); arXiv: 1909.01255.
23. M. E. Sachkov, A. S. Rastorguev, N. N. Samus', and N. A. Gorynya, Astron. Lett. **24**, 377 (1998).
24. M. Jurkovic, L. Szabados, J. Vinkó, and B. Csák, Astron. Nachr. **328**, 837 (2007); arXiv: 0705.2389.
25. T. Prusti, J. H. J. de Bruijne, A. G. A. Brown, A. Vallenari, C. Babusiaux, C. A. L. Bailer-Jones, U. Bastian, M. Biermann, D. W. Evans, et al. (Gaia Collab.), Astron. Astrophys. **595**, A1 (2016); arXiv: 1609.04153.
26. A. G. A. Brown, A. Vallenari, T. Prusti, J. H. J. de Bruijne, C. Babusiaux, M. Biermann, O. L. Creevey, D. W. Evans, L. Eyer, et al. (Gaia Collab.), Astron. Astrophys. **649**, A1 (2021); arXiv: 2012.01533.
27. A. Vallenari, A. G. A. Brown, T. Prusti, J. H. J. de Bruijne, F. Arenou, C. Babusiaux, M. Biermann, O. L. Creevey, C. Ducourant, et al. (Gaia Collab.), Astron. Astrophys. **674**, A1 (2023); arXiv: 2208.00211.

28. C. A. L. Bailer-Jones, J. Rybizki, M. Fouesneau, M. Demleitner, and R. Andrae, Astron. J. **161**, 147 (2021); arXiv: 2012.05220.
29. A. C. Robin, C. Reylé, S. Derriére, and S. Picaud, Astron. Astrophys. **409**, 523 (2003).
30. A. C. Robin, C. Reylé, J. Fliri, M. Czekaj, C. P. Robert, and A. M. M. Martins, Astron. Astrophys. **569**, A13 (2014); arXiv: 1406.5384.
31. O. Bienaymé, A. C. Robin, and B. Famaey, Astron. Astrophys. **581**, A123 (2015); arXiv: 1508.01682.
32. J. G. Fernández-Trincado, D. Minniti, E. R. Garro, and S. Villanova, Astron. Astrophys. **657**, A84 (2022); arXiv: 2111.04151.
33. Y. Tarricq, C. Soubiran, L. Casamiquela, T. Cantat-Gaudin, L. Chemin, F. Anders, T. Antoja, M. Romero-Gómez, F. Figueras, C. Jordi, et al., Astron. Astrophys. **647**, A19 (2021); arXiv: 2012.04017.
34. J. Holmberg, B. Nordström, and J. Andersen, Astron. Astrophys. **501**, 941 (2009); arXiv: 0811.3982.
35. T. Maas, S. Giridhar, and D. L. Lambert, Astrophys. J. **666**, 378 (2007); arXiv: 0706.2029.
36. V. Kovtyukh, I. Yegorova, S. Andrievsky, S. Korotin, I. Saviane, B. Lemasle, F. Chekhonadskikh, and S. Belik, Mon. Not. R. Astron. Soc. **477**, 2276 (2018).
37. A. L. Luo, Y. H. Zhao, G. Zhao, et al., VizieR On-line Data Catalog V/156 (2022).
38. R. E. Luck and D. L. Lambert, Astron. J. **142**, 136 (2011); arXiv: 1108.1947.
39. M. Meakes, G. Wallerstein, and J. F. Opalko, Astron. J. **101**, 1795 (1991).
40. Online Stilism 3D Map, Structuring by Inversion the Local Interstellar Medium. https://stilism.obspm.fr/. Accessed March 19, 2018.
41. R. Lallement, J. L. Vergely, B. Valette, L. Puspitarini, L. Eyer, and L. Casagrande, Astron. Astrophys. **561**, A91 (2014); arXiv: 1309.6100.
42. L. Capitanio, R. Lallement, J. L. Vergely, M. Elyajouri, and A. Monreal-Ibero, Astron. Astrophys. **606**, A65 (2017); arXiv: 1706.07711.
43. R. Lallement, C. Babusiaux, J. L. Vergely, D. Katz, F. Arenou, B. Valette, C. Hottier, and L. Capitanio, Astron. Astrophys. **625**, A135 (2019); arXiv: 1902.04116.
44. A. A. Henden, Mon. Not. R. Astron. Soc. **192**, 621 (1980).
45. T. J. Moffett and T. G. Barnes III, Astrophys. J. Suppl. Ser. **55**, 389 (1984).
46. L. Eyer, M. Audard, B. Holl, L. Rimoldini, M. I. Carnerero, G. Clementini, J. de Ridder, E. Distefano, D. W. Evans, P. Gavras, et al., Astron. Astrophys. **674**, A13 (2023); arXiv: 2206.06416.
47. A. S. Rastorguev, M. V. Zabolotskikh, and N. A. Gorynya, Astrophys. Bull. **79**, 629 (2024).
48. L. A. Balona, Mon. Not. R. Astron. Soc. **178**, 231 (1977).
49. A. S. Rastorguev, M. V. Zabolotskikh, Y. A. Lazovik, N. A. Gorynya, and L. N. Berdnikov, Astrophys. Bull. **77**, 144 (2022).
50. T. G. Barnes and D. S. Evans, Mon. Not. R. Astron. Soc. **174**, 489 (1976).
51. A. S. Rastorguev and A. K. Dambis, Astrophys. Bull. **66**, 47 (2011); arXiv: 1011.3305.
52. A. M. Cherepashchuk, *Close Binary Stars* (Fizmatlit, Moscow, 2013), Vol. 1 [in Russian].
53. O. Demircan and G. Kahraman, Astrophys. Space Sci. **181**, 313 (1991).
54. S. Wang and X. Chen, Astrophys. J. **877**, 116 (2019); arXiv: 1904.04575.
55. E. E. Mamajek, A Modern Mean Dwarf Stellar Color and Effective Temperature Sequence. https://www.pas.rochester.edu/~emamajek/EEM_dwarf_UBVIJHK_colors_Teff.txt. Accessed April 16, 2022).
56. P. P. Eggleton, Astrophys. J. **268**, 368 (1983).
57. M. S. Zverev, B. V. Kukarkin, D. Y. Martynov, P. P. Parenago, N. F. Florya, and V. P. Tsesevich, *Variable Stars* (Gostekhizdat, Moscow, 1947), Vol. 3 [in Russian].
58. A. Dotter, Astrophys. J. Suppl. Ser. **222**, 8 (2016); arXiv: 1601.05144.
59. I. Barnes, G. Thomas, T. J. Moffett, and M. H. Slovak, Astrophys. J. Suppl. Ser. **66**, 43 (1988).
60. J. Vinko, N. Remage Evans, L. L. Kiss, and L. Szabados, Mon. Not. R. Astron. Soc. **296**, 824 (1998).

Translated by A. Kolemesin